

Meteorological forcing of sea ice concentrations in the southern Beaufort Sea over the period 1979 to 2000

David G. Barber and John M. Hanesiak

Centre for Earth Observation Science, Faculty of Environment, University of Manitoba, Winnipeg, Manitoba, Canada

Received 1 July 2003; revised 23 February 2004; accepted 6 April 2004; published 12 June 2004.

[1] Northern Hemisphere sea ice areal extent, and perhaps thickness, have shown a detectable reduction over the past several decades. This situation is particularly apparent in the southern Beaufort Sea. The region encompassing the Mackenzie Shelf, the Cape Bathurst Polynya, and the Canada Basin mobile pack ice all occur in a region referred to here as the Canadian Arctic Shelf Exchange study area (CASES). In this paper we present results from an analysis of atmosphere, sea ice, and ocean coupling over the period 1979 to 2000 as a means of setting a physical science context for the CASES research network (operating over the period 2001–2005). Results show that the Cape Bathurst Polynya complex can be considered as a recurrent polynya; particularly the flaw leads associated with the early opening of the polynya. The Polynya appears to be a consequence of the Beaufort Sea Gyre acting like an ice bridge and a series of flaw leads creating conditions conducive to oceanic upwelling. The sea ice average areal extent has been decreasing in this region over the period 1979 to 2000. Large regional reductions are found (1) north of the Yukon and Alaska Coasts in the region between the Canada Basin pack ice and the landfast sea ice and (2) at the eastern limit of the Cape Bathurst Polynya in Amundsen Gulf. The meteorological forcing of sea ice anomalies occurs through a full range of timescales and space scales. At hemispheric scales a statistical cross-correlation analysis between weekly sea ice concentration anomalies and the Arctic Oscillation accounts for a maximum of about 25 percent of the explained variance and show a surprising spatial coherence in correlation magnitudes both within the study area and northward along the Canadian Archipelago coast. At local scales, positive and negative concentration anomaly periods can be explained through local-scale advective processes associated with regional-scale sea level pressure, 500 hPa geopotential heights, and surface temperature anomalies. *INDEX TERMS*: 1620 Global Change: Climate dynamics (3309); 3360 Meteorology and Atmospheric Dynamics: Remote sensing; 3349 Meteorology and Atmospheric Dynamics: Polar meteorology; 4540 Oceanography: Physical: Ice mechanics and air/sea/ice exchange processes; 9315 Information Related to Geographic Region: Arctic region; *KEYWORDS*: sea ice concentration anomalies, meteorological forcing, southern Beaufort Sea, Cape Bathurst Polynya, Arctic Oscillation, Arctic climate change

Citation: Barber, D. G., and J. M. Hanesiak (2004), Meteorological forcing of sea ice concentrations in the southern Beaufort Sea over the period 1979 to 2000, *J. Geophys. Res.*, 109, C06014, doi:10.1029/2003JC002027.

1. Introduction

[2] The western Canadian Arctic, the southern Beaufort Sea and the Mackenzie Valley are areas which have shown a dramatic increase in surface temperature over the past several decades [Comiso, 2003; Intergovernmental Panel on Climate Change, 2001]. The response of sea ice to these observed changes in local, regional and hemispheric-scale forcing is important to local peoples, marine ecosystems and northern development. In this paper we examine sea ice concentration changes over the period 1979 to 2000 as a means of assessing the spatial and temporal response of sea

ice to changes in atmospheric and oceanic forcing in this region. This will provide a historical context for the Canadian Arctic Shelf Exchange Study (CASES) field research program being conducted in this region between 2001 and 2005.

[3] For purposes of organization, we categorize the sea ice in the CASES study region into three “regimes”: (1) The offshore pack ice (A in Figure 1) consists of mobile annual and multiyear sea ice which occurs in regions beyond the extent of the maximum landfast ice. (2) The landfast sea ice (B in Figure 1) forms annually within the coastal margins over the continental shelves. (3) The Cape Bathurst Polynya complex (C in Figure 1). This Polynya complex consists of a series of flaw leads and a sensible/latent heat polynya within Amundsen Gulf. The flaw lead

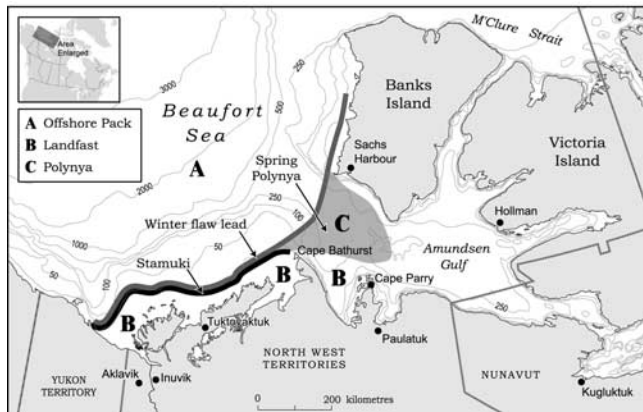


Figure 1. The CASES study region showing the location and shape of the three sea ice regimes considered here.

polynya system is located (on average) at the shelf break between Amundsen Gulf and the Beaufort Sea (Figure 1) and is a recurrent polynya in that these flaw leads appear to occur annually. The recurrence of the flaw leads is due to the central pack ice acting like an ‘ice bridge’ in the classical notion of an ice bridge holding back sea ice from advecting into a region (see, for example, *Barber et al.* [2001] with reference to the NOW polynya).

[4] A significant interface feature is formed at the confluence of the offshore pack and the landfast ice region north of the Mackenzie estuary and the Tuktoyuktuk peninsula (Figure 1). This region produces a highly deformed shear zone where the anticyclonic rotation of the offshore pack compresses the advancing edge of the landfast sea ice. The compression ridges (termed “stamukhi” by local Inuvialuit) in this area can be large, often exceeding several meters in the sail and keel. The stamukhi acts as a barrier to the freshwater flux from the Mackenzie in the winter thereby forming an inverted lake which has been named Lake Harlinveaux, in honor of the first western scientist to document the importance of this geophysical feature [*Carmack and Macdonald*, 2002].

[5] The offshore pack responds to synoptic-scale atmospheric patterns such as the Arctic Oscillation (AO) and the North Atlantic Oscillation (NAO), each of which are manifestations of the Northern Annular Mode (NAM). In each case, indices have been computed to show the strength of oscillatory patterns of high and low-pressure systems affecting particular areas [see, e.g., *Proshutinsky and Johnson*, 1997; *Thompson and Wallace*, 1998; *Hurrell et al.*, 2001; *Overland and Adams*, 2001; *Krahmann and Visbeck*, 2003; *Visbeck et al.*, 2003].

[6] Because of the synoptic setting, the pack ice of the Beaufort Sea generally rotates in an anticyclonic gyre (clockwise in the northern hemisphere) centered near 78°N and 150°W. This anticyclonic flow is due to a predominant surface high-pressure system over the region in winter. In the winter the seasonal pack within the transition zone (defined as the low concentration areas between the landfast ice and the offshore pack) is incorporated into the gyre and rotates at about 35° to 45° per year. This average circulation is responsible for much of the export of sea ice from the Canada Basin into the transpolar

drift and ultimately the export through Fram Strait [*Kwok and Rothrock*, 1999]. The gyre also accounts for significant deformation induced increases in ice volume in this region [*Melling and Riedel*, 1996]. The surface waters of the Canada Basin are known to originate in the Pacific [*Carmack and Macdonald*, 2002], whereas the deeper waters (>200 m) originate in the Atlantic. These deeper waters circulate in a counterclockwise (cyclonic) flow opposite to the sea ice [*Carmack and Macdonald*, 2002].

[7] *Parkinson et al.* [1999] showed that between 1978 and 1998 there was an annual average reduction of about 34,600 km² in the areal extent of sea ice over the northern hemisphere. This reduction was spatially heterogeneous with larger decreases in particular locations (e.g., Chukchi and Laptev Seas) and slight increases in extent in other regions (e.g., Baffin Bay). The issue of a reduction in ice thickness (volume) is more controversial in the sense that observations from submarine sonar data suggests a decline in thickness over the past 40 years [*Rothrock et al.*, 1999] but this may be due more to a sampling issue than a real reduction in the mass balance of the sea ice [*Holloway and Sou*, 2002].

[8] Recent evidence suggests that sea ice areal extent continues to decline. In 2002 the minimum extent and area of sea ice was observed for the Arctic Basin since the passive microwave remote sensing record began in 1978 [*Serreze et al.*, 2003]. The reduction was due to anomalously strong southerly winds in spring which advected sea ice poleward in the Siberian sector of the arctic. A persistent low-pressure system and high air temperatures promoted divergence in the pack ice (decreasing albedo) thereby enhancing melt. The divergence of the sea ice also promoted development of early flaw leads at the continental shelf breaks along the western sector of the Arctic Basin which may have impacted the overall reduction in areal extent by limiting ice growth in the late winter and promoting ablation in the spring and summer [*Serreze et al.*, 2003]. Under strong positive AO conditions we would expect the early formation of shore flaw leads and advection of ice away from the coasts under a predominantly cyclonic flow in the atmosphere [*Drobot and Maslanik*, 2003]. Although the observations of areal extent are somewhat consistent with the theory of the AO postulated by *Rigor et al.* [2002] the authors note that there were distinct differences in the interpretation of the sea ice anomalies relative to both a weak AO index early in the spring and winter preconditioning of this event [*Serreze et al.*, 2003].

[9] Much of the work described above has used the passive microwave sea ice record which now spans 1978 to 2004. Precision of passive microwave derived ice concentrations is relatively high (5% ~ 10%) and stable during the dry seasons (i.e., winter) [*Steffen et al.*, 1992] and generally lower (10% ~ 15%) and more variable during the wet seasons (i.e., summer) [*Emery et al.*, 1991]. More specifically, in summer, the NASA Team algorithm showed a lack of agreement with Landsat of 11.0 (±22.9%) [*Steffen and Schweiger*, 1991], with AVHRR of 3.1 (±8.8) [*Emery et al.*, 1994], but underestimated from 20.4% (±7.1%) to 33.5% (±28.1%) in comparison with ice charts [*Agnew and Howell*, 2003]. The reason for the large range in precisions in the summer is partly due to the important role water in liquid phase plays on surface/volume dielectrics

(and thus emission), and partly an artifact of the comparison of two stochastic estimates with neither one being “truth.” In this paper we use sea ice concentration anomalies which are computed for any particular week minus the grand average of all the years of that week. This means that if the passive microwave record systematically over or under estimates concentration (either in space or time), the anomaly will be robust to this bias (i.e., the anomalies have good relative precision). We also limit our interpretation to anomalies which are greater than ± 5 percent thereby focusing on strong temporal and spatial patterns.

[10] Although not perfect, our only tools for projecting future sea ice conditions are through the use of regional, hemispheric and global circulation models. Climate change projections from the Canadian Centre for Climate Modeling and Analysis (CCCMA) indicate a reduction in sea ice in both the Northern and Southern Hemispheres. Although differences exist between different versions of their global model, both show a historical reduction that is broadly consistent with the passive microwave observational record [Flato and Boer, 2001]. Projections suggest that the NH sea ice reduction would result in a seasonally ice-covered Arctic as early as 2050. Maximum winter extent declines more slowly than the summer minimum, with a reduction of 10–20% by 2050 (G. M. Flato, personal communication). Research using a variety of GCMs have shown a reasonable level of agreement between observations and modeling within recent decades [Vinnikov *et al.*, 1999]. If these projections are even close to correct it means we can expect significant changes in the arctic system and its coupling to the rest of the planet.

[11] Our objective in this paper is to investigate linkages between sea ice concentration anomalies and atmospheric forcing in the southern Beaufort Sea. More specifically, we examine four interrelated research questions: (1) What are the average patterns of sea ice formation and decay within the region? (2) Is there evidence of hemispheric connections between local sea ice concentration anomalies and the AO? (3) Is there evidence of local-scale atmospheric or oceanic forcing of observed strong positive and/or negative sea ice concentration anomaly periods? (4) Are there consistent spatial and/or temporal trends in sea ice concentration anomalies and can these be explained through the development of associations raised in the second and third research questions?”

2. Methods

[12] The historical atmospheric analysis used daily NCEP (National Center for Environmental Prediction) gridded atmospheric fields between 1979 to 2000 that included surface air temperature (2 m), sea level pressure (SLP), and 500 hPa geopotential heights [Kalnay *et al.*, 1996]. Atmospheric variables were extracted from an area 60°N to 90°N latitude and 180°W to 70°W longitude to indicate large-scale atmospheric patterns associated with the local area. Details of the general synoptic climatology of the region, including surface observations of coastal stations are given by Barber *et al.* [2003].

[13] The data were averaged to depict overall mean, annual and monthly atmospheric conditions. Mean atmospheric fields spanning all available years were calculated

for each variable to inspect overall climatological conditions and individual annual means to illustrate interannual variations. The data were also averaged into 13 months (year months) each consisting of 4 year weeks (28 days), except year month 13 which contained one extra day (last day of the year). Leap year days were added into the year week containing that day. Monthly data were averaged in two ways: (1) monthly means spanning all years to illustrate overall seasonal trends and (2) monthly averages for each individual year to inspect intraannual variations.

[14] Sea ice concentrations were provided by the EOS Distributed Active Archive Center (DAAC) at the National Snow and Ice Data Center (NSIDC), University of Colorado, Boulder, Colorado. The data were derived from Nimbus 7 Scanning Multi channel Microwave Radiometer (SMMR) and DMSF-F8, -F11 and -F13 Special Sensor Microwave Imager (SSM/I) daily brightness temperatures at a grid cell size of 25×25 km. The sea ice concentrations were generated by the Oceans and Ice Branch, Laboratory for Hydrospheric Processes at NASA’s Goddard Space Flight Center (GSFC), using SMMR brightness temperatures that were processed at NASA GSFC and SSM/I brightness temperatures processed at the NSIDC. Sea ice concentration retrievals were based on the NASA team algorithm. The data cover the period January 1979 through January 2000.

[15] The data were distributed by NSIDC as daily composites from which we computed weekly averages. The Year Week and Year Month schemes were also used to structure the sea ice data into a consistent time series. Spatially, the data depicted the study area in a 85 by 85 array, with each pixel having a nominal spacing of 25 km^2 . Each pixel was coded to either land or ice concentration (in percent). Weekly averages resulted in 1144 of these images ($52 \times 22 = 1144$). The data were coregistered into a single three dimensional array with coordinates defined as (i, j, and t). Sea Ice concentration pixels located within one pixel of land were removed from subsequent analysis due to the potential of land contamination in the retrieval algorithm. Computations varied depending on the particular objective being addressed, as follows.

[16] We computed a 22 year weekly averaged data set. This resulted in an average ice concentration for a week which was computed as the average of the 22 years of that week. The product of the data manipulation was a data set of 52 weekly averages. We extracted a subset of these data for visual presentation and an animation of the weekly average ice concentrations was produced (available at <http://www.umanitoba.ca/ceos/iceanimations>). To estimate the average timing of formation and decay within the CASES study region we produced a data set by defining the first date at which the concentration of sea ice reached a threshold. The formation images were created by assigning the value of the first week of the year in which a pixel reached or exceeded an ice concentration value of 70%. The range of weeks searched was limited to week 35 of a given year through to week 8 of the following year (this ensured that we selected only the 70% ice formation point and not the corresponding decay point). The decay images were created by assigning the value of the first week of the year in which a pixel had an ice concentration value less than or equal to 30%. We also computed the standard deviation of these formation and decay images to illustrate the local

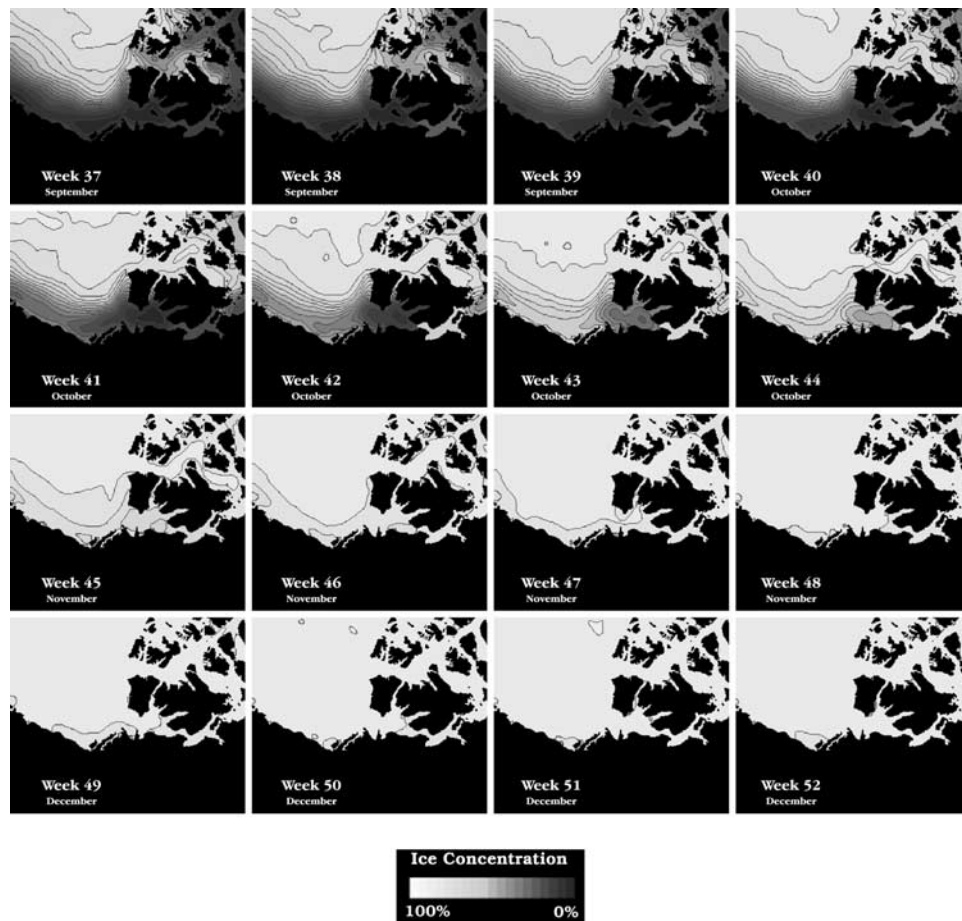


Figure 2. Average sea ice concentrations during freeze-up (formation) computed over the period 1979 to 2000 for weeks 37 to 52. Concentrations are expressed in percent.

variability. The range of weeks searched was limited to week 9 to 34 of each particular year. The search of the last year of the data set was truncated at week 52, since there were no data available for the following year.

[17] We computed a 22 year time series using the weekly anomalies from the full data record. The methods of computation were identical for both the monthly and weekly anomalies. Details of the numerical computations are available elsewhere [Barber *et al.*, 2001]. We do not interpret sea ice concentration anomalies smaller than $\pm 5\%$ since this level is likely within the noise of the ice concentration retrieval algorithm [Steffen and Schweiger, 1990].

[18] Weekly averages of the Arctic Oscillation index were computed on the basis of data available through the University of Washington (available at http://jisao.washington.edu/data/annularmodes/data/ao_index.html). Daily data were averaged to weekly for the period 1979 to 2000 following the same procedure as the Year Week computations done on the sea ice concentration anomalies. The AO weekly time series was then combined with sea ice concentration anomalies from all pixels within the study area to produce a cross-correlation surface (at lag 0). The magnitude of the correlation coefficient (ρ) was then plotted back into the study area frame to examine the spatial distribution of the correlation field. We also computed a seasonal separation of this correlation surface by examining

the cross correlations for two 6 month seasons: summer (weeks 18–39; approximately May–October) and winter (weeks 40–17; approximately November–April) with the corresponding seasons for sea ice concentration anomalies.

[19] To examine spatial trends in sea ice concentration anomalies we computed a time series slope surface for the study region using the 1144 weekly anomaly fields. For each pixel in the weekly deviation images, a time series was constructed which consisted of pixel (I, j) ordered by time. Since the size of the passive microwave data set was 85 by 85 pixels, thereby creating 7225 time series in total. A least squares linear regression line was fit through each time series and the probabilities associated with the confidence intervals for the slope were computed. A final image was constructed in which the value of each pixel of the image represented the slope of the time series at each of the 7225 pixel locations within the CASES study region. We retained those slopes which met or surpassed the 99 percent confidence level ($P < 0.01$). These slopes were then mapped back onto the passive microwave grid to show the spatial pattern of the slopes in ice concentration anomalies.

3. Results and Discussion

[20] The average cycle of sea ice formation from the passive microwave record (Figure 2) shows that ice grows

October to January

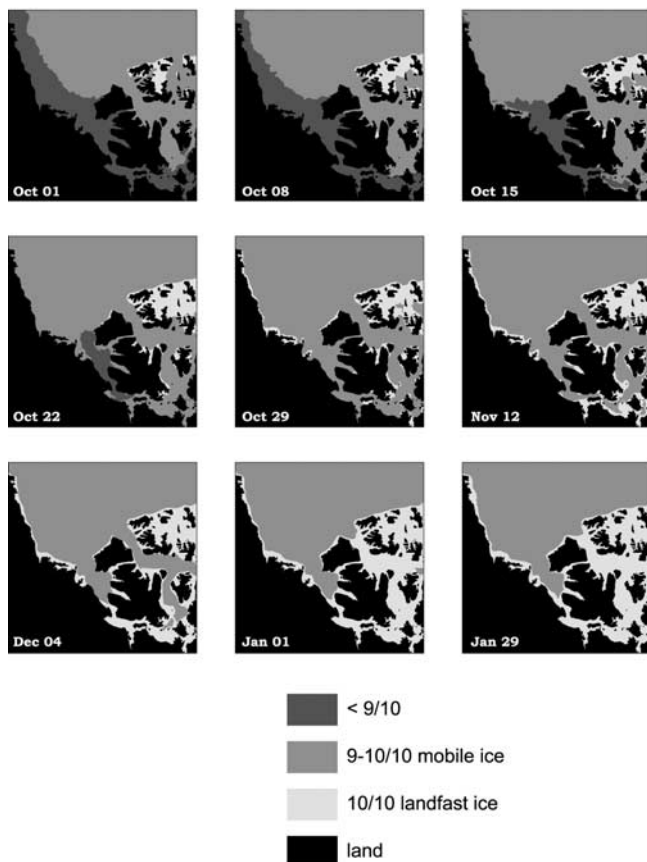


Figure 3. Sea ice concentrations for selected weeks from the Canadian Ice Service Digital ice chart products showing the median ice concentration (expressed in tenths) for mobile and landfast sea ice during freeze-up (formation).

southward, from the summer minimum extent of the central pack, beginning about the end of September (week 39). The southward progression occurs rapidly so that by week 43 (Figure 2) the ice arrives near the coast. The Cape Bathurst Polynya complex is the last area to form sea ice (weeks 42–44). The ice can remain mobile in the Polynya region well into the winter (approximately February) but the concentrations are high (10/10ths).

[21] Data from the Canadian Ice Service (CIS) digital ice charts provide a clear representation of the annual median concentrations of mobile and fast ice (<9/10, 9/10, 10/10 and landfast; Figure 3). Young ice forms along the pack ice margin in early October and by Oct 15 the new ice has met young ice forming in sheltered bays, progressing northward (Figure 3). Both dynamic and thermodynamic processes will give rise to an increase in ice volume during this period. By the end of October high concentrations of ice are present along the Mackenzie Shelf (October 29, Figure 3) and by November 12, the landfast ice has begun to grow in Franklin Bay and along the coast of Cape Parry. Over the December and January period the fast ice regions continue to grow outward from the coasts. These growth periods result in shear zone features where the mobile pack and the landfast ice meet.

These shear zones are clearly visible in satellite synthetic aperture radar (SAR) data (not shown here). The Canadian Ice Service chart data are derived from a composite of satellite and aircraft data and as such are not systematic in time, thus the unusual dates presented in Figure 3.

[22] Average annual decay of sea ice occurs with a time/space pattern which is quite different than formation (cf. Figures 2 and 4). The passive microwave record indicates some transient reductions in ice concentration in the areas where we would expect to find flaw leads, as early as week 14 (Figure 4, early April). Sustained reduction in concentrations occur by week 16 (again in the areas of the Banks and Mackenzie Shelf flaw leads). Three nodes of sustained ice reduction appear just west of Banks, north of the Tuk Peninsula and in the eastern limit of Amundsen Gulf by about week 20 (Figure 4). These nodes interconnect in the subsequent weeks to produce a distinctive polynya complex with a limb along the shelf/slope break in the approximate locations of the flaw lead polynyas and with a limb into Amundsen Gulf (compare across weeks 20 to 26; Figure 4). This “tri-node” polynya complex then advances in size throughout the spring melt to a point where ice free water exist most of the way along the Alaskan Coast (week 34; Figure 4).

[23] Analysis of the corresponding Canadian Ice Service (CIS) data shows a very similar pattern of reduction in ice concentration. The first reduction in the median concentration occurs in the flaw lead polynya north of the Tuk Peninsula (May 14; Figure 5). The Banks Island flaw lead polynya is then evident by May 28 with both of these flaw leads joining by mid June (Figure 5). A similar “tri-node” shape is evident in the CIS median concentration data over the period mid-June to early July (Figure 5). The dates of the CIS estimated median opening of the flaw lead polynya system and that from passive microwave record are not exact but indicates that the flaw leads open, on average, as early as May 1. A recent overpass of the NOAA AVHRR sensor confirms that in fact the flaw lead polynya system was well developed by May 1 of 2002. Under conditions of a sustained easterly flow in April the central pack shifted west, opening a long flaw lead along the western margin of Banks Island (Figure 6).

[24] On average, the region closes (formation) with a spatial pattern which indicates rapid growth south from the central pack (week 36 to 41; Figure 7a). Formation in the polynya complex occurs somewhat later (week 43; Figure 7a). The pattern of the growth is clearly one of advancing formation from the north toward the south, until the coast is reached, then continued ice formation SE into Amundsen Gulf. The dates of average decay show the pattern of the tri-node polynya shape described above, with decay as early as weeks 24 to 26 (Figure 7a) in the nodes, with continued decay toward the NW along the coast, propagating northward as the central pack retreats (Figure 7a).

[25] Interannual variability in these average formation and decay patterns indicate a number of interesting features which may lead us to a better understanding of the processes controlling both dynamic and thermodynamic characteristics of the sea ice. The standard deviation (SD)

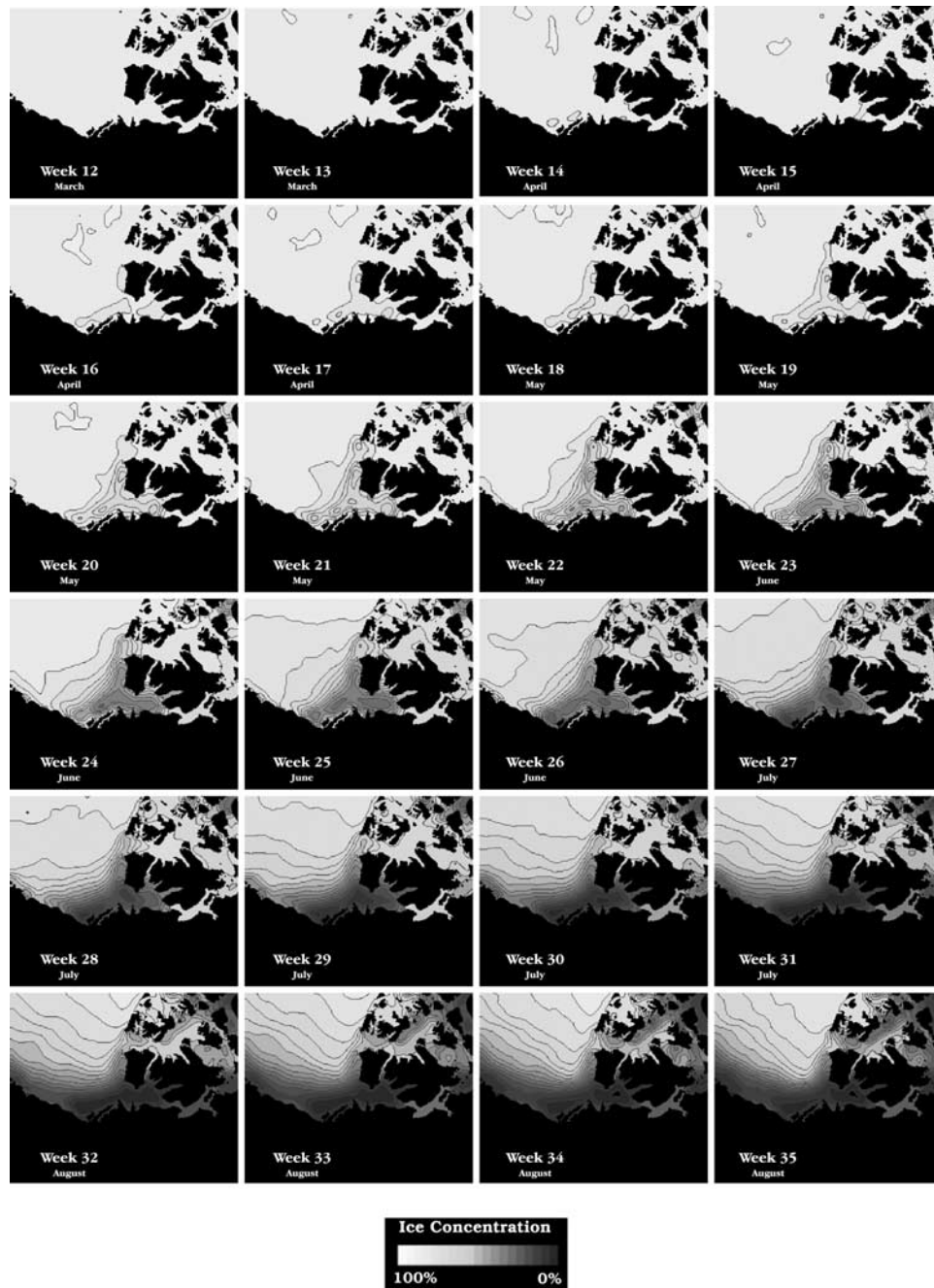


Figure 4. Average sea ice concentrations during breakup (decay) averaged over the period 1979 to 2000 for weeks 12 to 35. Concentrations are expressed in percent.

indicates that the variability in the week of formation date is smallest nearest to the central pack and the landfast ice ($SD = 1$; Figure 7b), twice as large in the region between the landfast ice and the offshore pack ($SD = 2$) and largest ($SD = 3$) in the region of the Banks Island flaw lead. We speculate that this result is due to the fact that during the period of formation thermodynamic processes dominate over dynamic ones near the margin of the central pack and in the near shore areas (i.e., the ice grows thermodynamically more quickly than it moves). At the interface between the pack and the landfast ice we can expect a larger variability in formation due to the fact that the

central pack can move across the pole in response to different hemispheric teleconnections. The landfast ice will grow until it approaches the shelf break region at about 20 m ocean depth. Variability in air temperature will cause variability in the timing of this formation and the presence of open water between the pack and the fast ice can produce upwelling when favorable winds occur. The high variability in the flaw lead is likely due to oscillations of the central pack toward and away from Banks Island. As expected, the standard deviation in the decay pattern confirms that the polynya region has the highest variability in decay (Figure 7b).

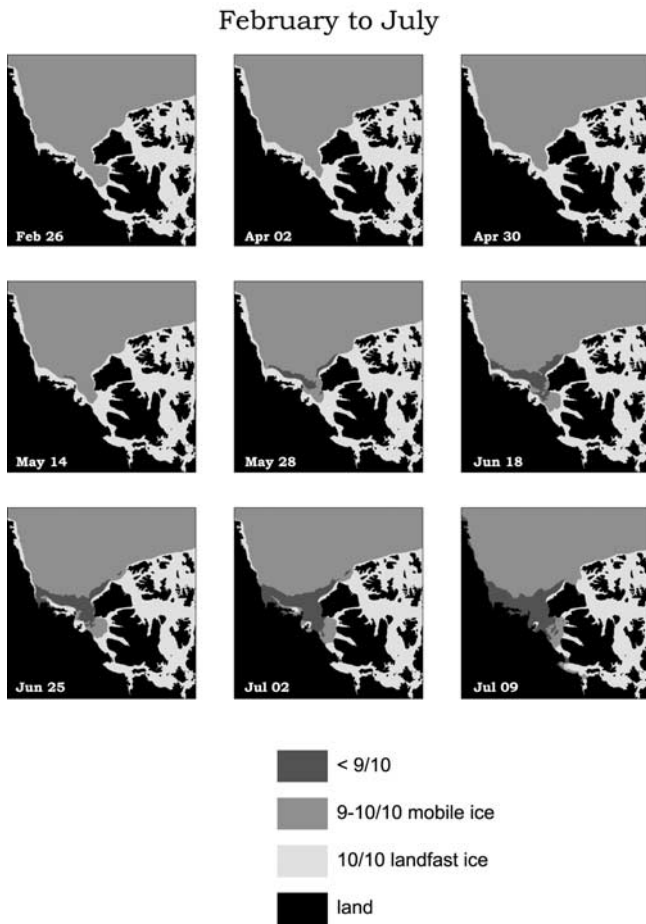


Figure 5. Sea ice concentrations for selected weeks from the Canadian Ice Service Digital Ice Chart products showing the median ice concentration (expressed in tenths) for mobile and landfast sea ice during breakup (decay).

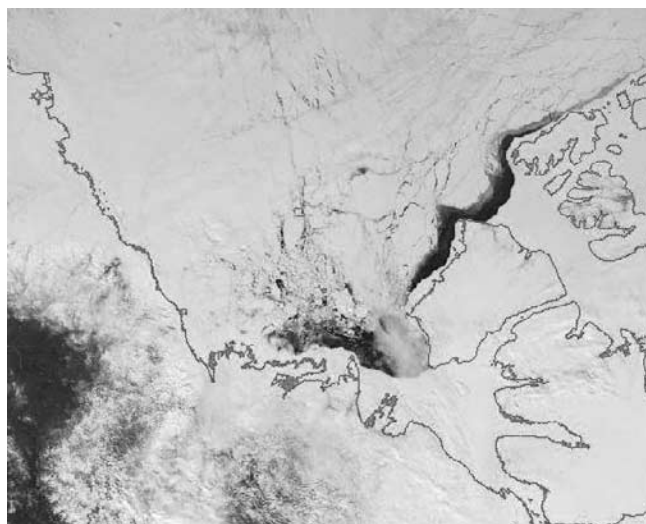


Figure 6. NOAA AVHRR image of the southern Beaufort Sea including the CASES study region for 1 May 2000. Open water is depicted by dark shading and sea ice is depicted by light shading; land masks indicate geographic location. The flaw lead polynya system is clearly evident west of Banks Island as are leads and cracks in the central arctic pack.

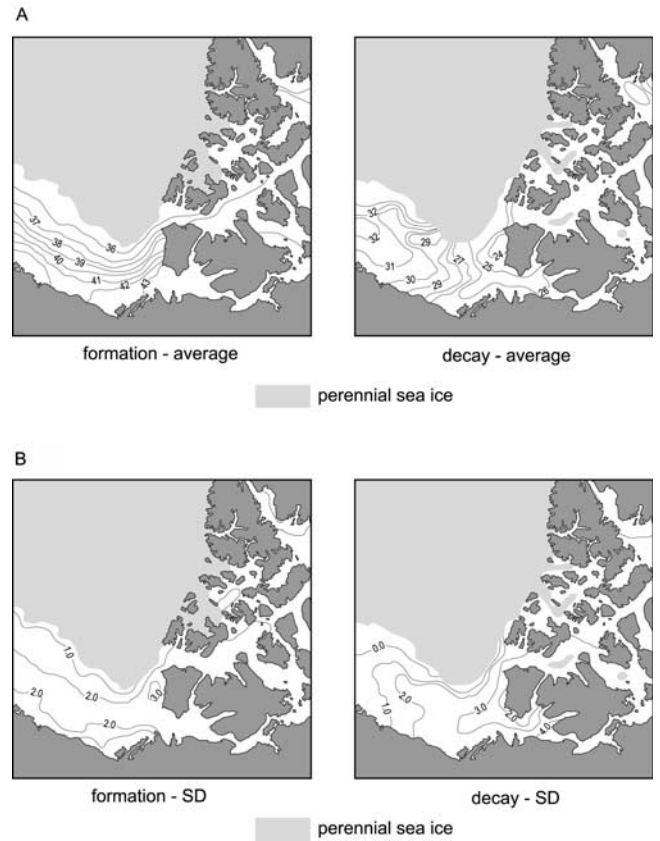


Figure 7. (a) Average date, expressed in week number, for the formation of sea ice (defined as >70 percent concentration) and decay (defined as <30 percent) averaged over the period 1979 and 2000. (b) The standard deviations of these average dates of formation and decay show the interannual variability or variance in these average weeks.

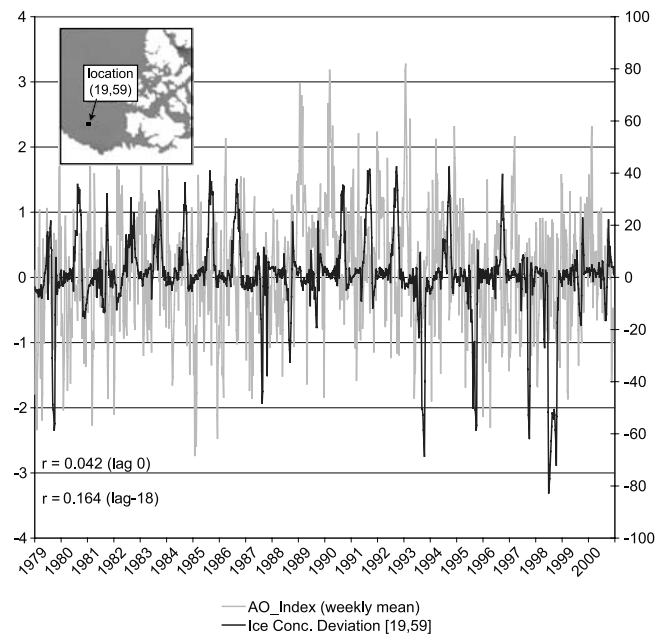


Figure 8. Time series plot of the weekly Arctic Oscillation and one pixel of sea ice concentration anomalies (location 19, 59) for the period 1979 to 2000. The correlation coefficient for this cross-correlation (lag 0) is 0.042.

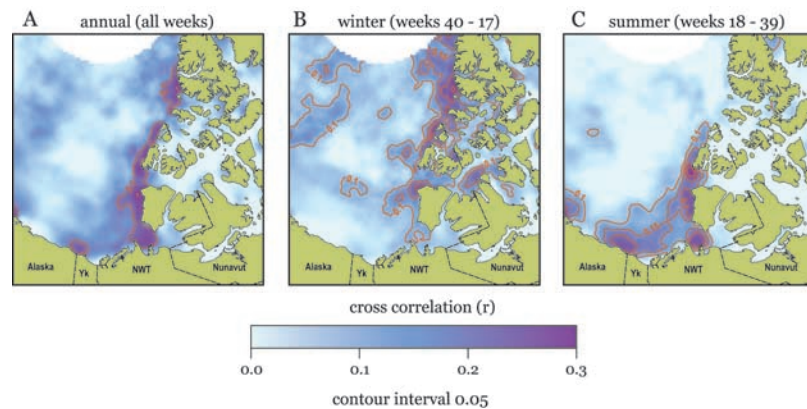


Figure 9. Correlation surface showing the magnitude and spatial coherence of correlation coefficients for each pixel in the study area frame. The computations are done for each coordinate using the concentration anomaly series at that location and the AO time series for the region (see Figure 8). The spatial patterns of the correlations show where geographically we can expect to find the strongest relationship between sea ice concentration anomalies and the AO. (a) Full weekly, interannual data set. (b) Winter season (weeks 40–17; approximately November–April). (c) Summer season (weeks 18–39; approximately May–October).

[26] To investigate hemispheric forcing of sea ice we created a cross correlation surface between the weekly average of the AO time series and time series of sea ice concentration anomalies within the study area. An example of this computation is provided for one pixel located at (19c, 59r). The AO time series is quite noisy as is the sea ice concentration anomaly series (Figure 8). At a lag of zero the correlation coefficient for this series is very low (0.042) increasing to a maximum (0.164) at a lag of -18 weeks. For each sea ice concentration anomaly series in the study area we did a cross correlation (at lag 0) with the AO time series to examine the magnitude and spatial coherence which may be evident in such a correlation surface.

[27] The results show that the sea ice concentration anomalies are correlated and that there is spatial coherence in these correlations. The interannual weekly series shows the strongest correlation (about 15 to 20 percent of the explained variance) to be located along the Canadian Archipelago coast at the interface between the pack ice and the Cape Bathurst Polynya and the Mackenzie Shelf (Figure 9a). In winter we see the largest correlations in a region we would expect to find strong dynamic processes associated with the central pack circulation up against the NW portion of the Canadian arctic archipelago (Figure 9b) in response to winter time AO forcing as postulated by *Proshutinsky and Johnson* [1997]. The summer component shows generally higher correlation coefficients and indicates that the correlation is highest in the region where we would expect the most variability in summer concentrations of sea ice (Figure 9c). The location happens to coincide with the study area selected for the CASES research network including all three sea ice regimes examined in this paper. Overall, the magnitude of the correlations show that the AO is likely to explain something on the order of 20 to 30 percent of the observed variance in sea ice concentration anomalies. The spatial coherence of these correlations indicate that the NW margin of the Canadian Arctic Archipelago (winter) and the CASES study region (summer) are regions where we

can expect to see the strongest coupling between the AO and sea ice.

[28] To investigate regional forcing we extracted two periods of unusually strong positive and two strong negative sea ice concentration anomalies from the complete series. The periods chosen were (1) May 1 to October 3, 1983 (positive; Figure 10) and (2) May 1 to July 1, 2000 (positive; Figure 11); (3) May 1 to October 3, 1993 (negative; Figure 12) and (4) April 1 to November 1, 1998 (negative; Figure 13). Atmospheric anomalies were also generated with negative (positive) anomalies indicating smaller (larger) magnitudes than the norm computed against the same average climatology (1979–2000). Overall mean anomaly fields were also generated for each of the four years spanning the months over which the ice anomalies occurred (e.g., a mean SLP anomaly spanned May to October in 1993, etc.). This was done to observe long timescale atmospheric patterns associated with each ice anomaly period.

[29] Positive ice concentration anomalies are presented for 1983 (Figure 10) and 2000 (Figure 11). Higher than expected concentrations were found between about week 19 and week 41 (May to October, 1983). The positive anomalies were located within the Cape Bathurst Polynya complex in the early part of this period and along the Mackenzie shelf in the fall (Figure 10). In 2000, a shorter duration positive anomaly was identified between May 1 and July 1. This series also shows the positive anomalies located within Amundsen Gulf and the Cape Bathurst Polynya (Figure 11). Animations of the full time series anomalies and the extracted positive and negative anomaly periods are available at <http://www.umanitoba.ca/ceos/iceanimations>.

[30] The atmospheric influence on sea ice concentration anomalies is evident from mean sea level pressure (SLP), surface air temperature anomalies and 500 hPa geopotential height anomaly patterns (Figures 14a, 14b, and 14c). During positive sea ice anomalies a mean surface ridge resides over the southern Beaufort Sea and southern

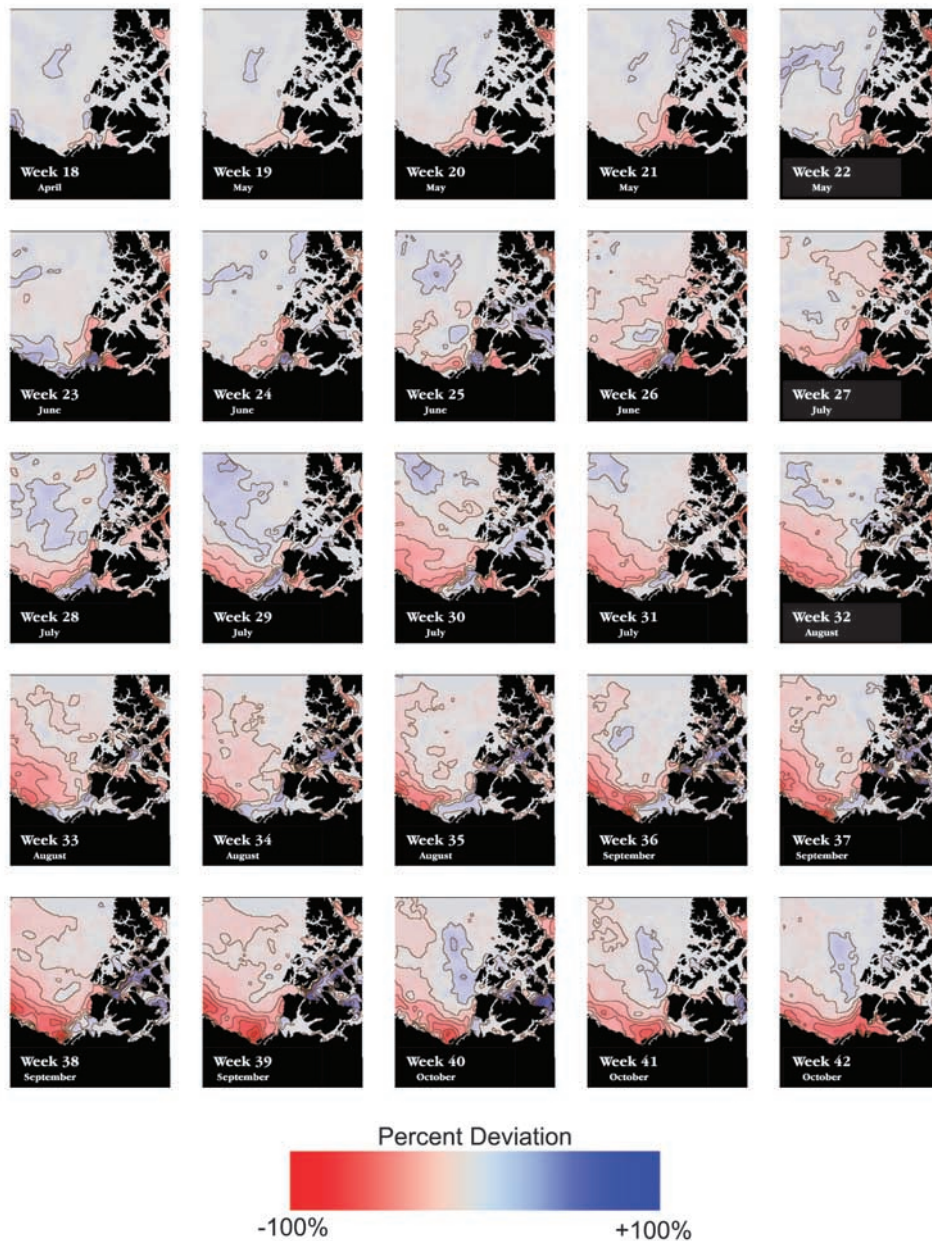


Figure 10. Selected positive concentration anomaly period from the end of April to the third week in October 1983 expressed as positive and negative sea ice concentration percent relative to the average between 1979 and 2000.

Nunavut (Figure 14a). This ridge pattern developed sooner (a few weeks to more than a month) than the initiation of the ice anomaly, suggesting that the atmosphere is the key mechanism behind the positive ice anomalies. The SLP pattern induced a mean NE to east surface flow (sometimes from the SE). Corresponding overall mean air temperature anomalies were -1°C to -3°C over the CASES region with a cold source region to the SE (i.e., surface advection was from a cold anomaly source) (Figure 14b). In all negative (positive) ice anomaly cases, the source region was found to play an important role in

maintaining and prolonging cold air (warm air) temperature anomalies until the atmospheric circulation changed significantly to “kick” the ice regime into a more normal mode. The magnitude of the air temperature anomalies for years that produced positive ice anomalies were much more negative in spring and fall than for summer, suggesting that spring melt and fall freeze-up are the most important seasons for producing the ice anomalies. For both positive ice anomaly years, the overall mean 500 hPa pattern shows a distinct negative anomaly (with a cold upper trough or low) extending from the northern

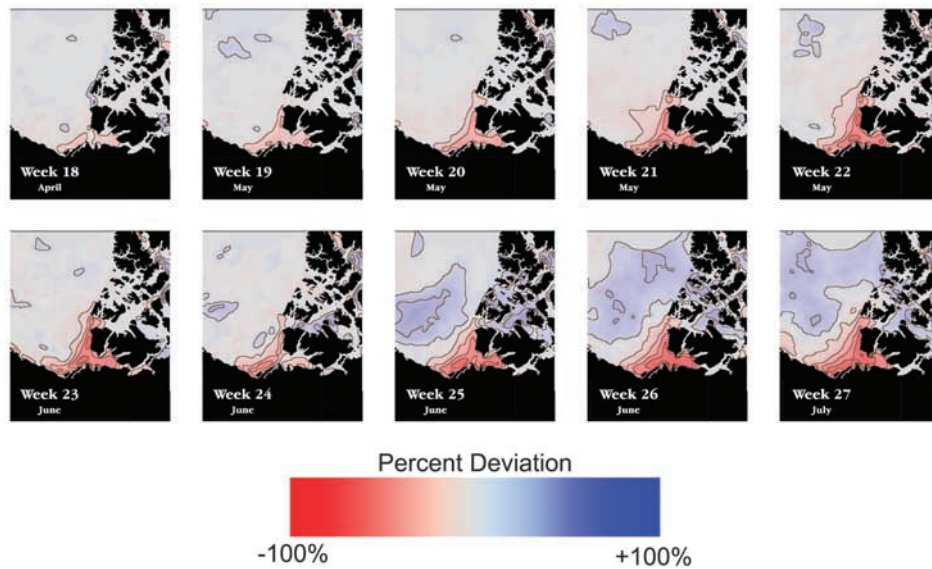


Figure 11. Selected positive concentration anomaly period from the first week in May to the first week in July 2000 expressed as positive and negative sea ice concentration percent relative to the average between 1979 and 2000.

Arctic Ocean down into the CASES, Yukon, and Mackenzie Regions (Figure 14c) and positive 500 hPa anomalies to the S and SE. The resulting 500 hPa pattern induces a strong west to NW cold flow aloft in the CASES region. See *Barber et al.* [2003] for further details.

[31] Negative ice concentration anomalies were identified in 1993 and 1998 (Figures 12 and 13). Lower than expected concentrations were found beginning about week 19 and continuing through week 27. These anomalies began inside Amundsen Gulf and appear to be associated with the Cape Bathurst Polynya (Figure 12). The negative anomalies tend to move westward throughout weeks 30 to 42 and are generally located between the central pack ice and the landfast sea ice north of the coast, west of the Mackenzie estuary, during the fall period (Figure 12). The anomalies again begin in the Polynya region (week 15; Figure 13) and continued to grow over the period until about week 22. A large negative concentration anomaly is clearly visible propagating westward over the period week 25 to 31 after which point the fall freeze-up shows a similar negative concentration anomaly due to the low amount of sea ice present at the beginning of the fall period (Figure 13). This 1998 sea ice season is described in detail elsewhere [*Maslanik et al.*, 1999].

[32] During negative sea ice anomalies (1993 and 1998), a mean surface ridge still resides near the CASES region but is shifted toward the east (Figure 14a). Again, this ridge pattern develops sooner (a few weeks to more than a month) than the initiation of the ice anomaly. The seasonal SLP pattern induces a mean easterly flow in Spring, south to SW flow in Summer and Fall (or SE flow with a warm source). Corresponding overall mean air temperature anomalies were $+1^{\circ}\text{C}$ to $+4^{\circ}\text{C}$ over the CASES region with a pronounced warm source region

to the E and SE in 1998 (i.e., surface advection was from a warm anomaly source; Figure 14b). The magnitude of the air temperature anomalies for years that produced negative ice anomalies were much more positive in Spring and Fall than for Summer, suggesting once again that Spring melt and Fall freeze-up are the most important seasons for producing the ice anomalies. In 1993, the overall mean 500 hPa pattern showed a distinct positive anomaly ridge extending from the northern Archipelago through the CASES region and into the Yukon/Alaska area (Figure 14c), whereas, in 1998 strong positive 500 hPa anomalies existed over the Archipelago accompanied by strong negative anomalies in the Bering Sea. The resulting 500 hPa pattern induces a weak NW flow aloft in the CASES region (not shown).

[33] The interpretation of the atmospheric controls on generating these sea ice concentration anomalies should be interpreted as illustrative rather than conclusive as it is likely that different ensembles of atmospheric forcing variables could result in the same observed sea ice concentration deviation pattern, and visa versa.

[34] When one examines the full sea ice concentration anomaly data set it is apparent that there is a significant amount of variation over various space and timescales. One way to present trends in these anomalies is to compute the slopes of a least squares line through the monthly time series of the anomalies. Figure 15 provides an illustration of one such anomaly time series for the pixel location (12r, 58c). The time series of the anomalies indicates a tendency for more positive anomalies in the 1980's and more negative anomalies in the 1990s. This general observation is consistent with other researchers who have discovered various timescales of variability corresponding to the decade of the 80's versus those in the 90's [e.g., *Proshutinsky and Johnson*, 1997; *Rigor et al.*, 2002; *Drobot and Maslanik*, 2003]. It is

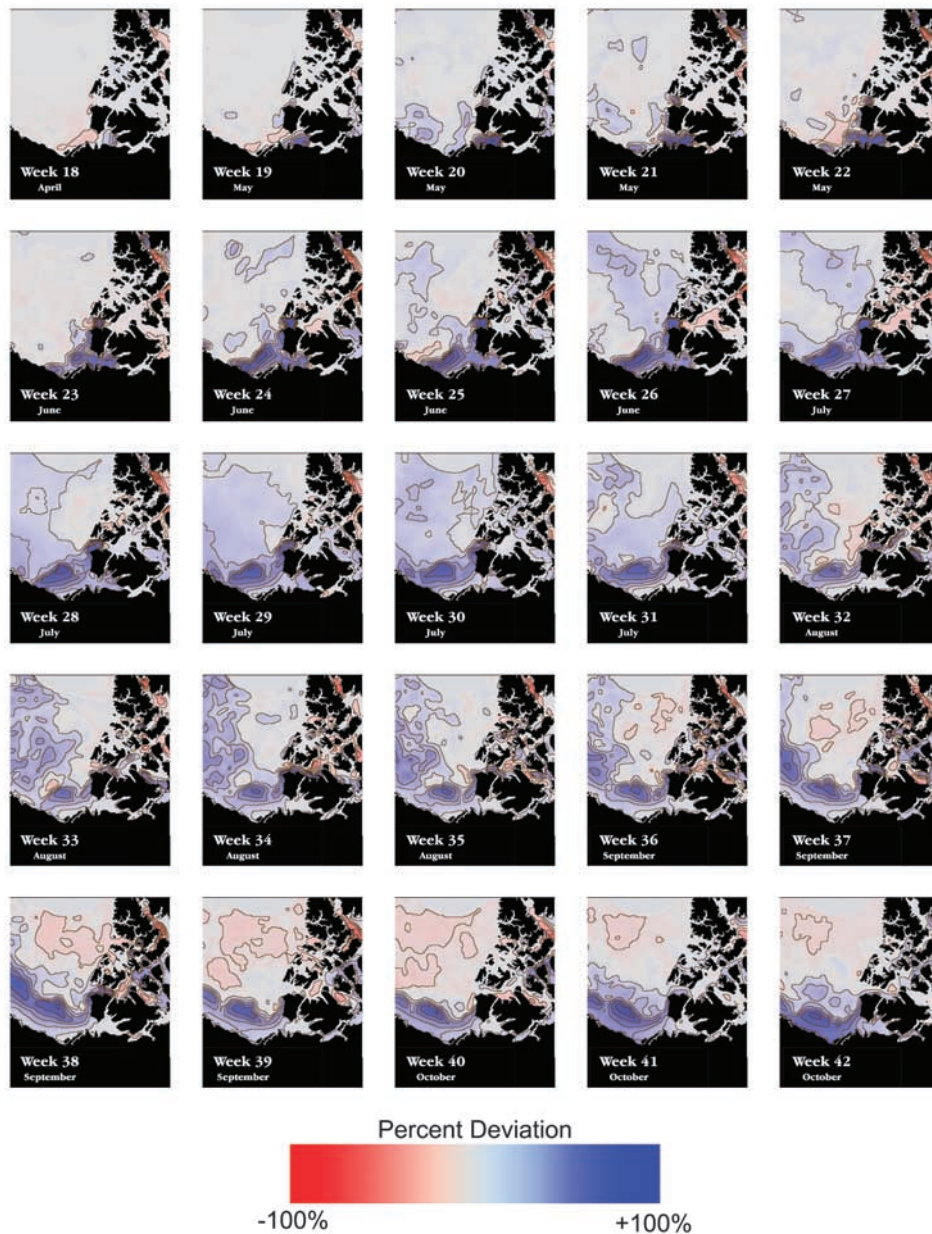


Figure 12. Selected negative concentration anomaly period from the first week in May to the third week in October 1993 expressed as positive and negative sea ice concentration percent relative to the average between 1979 and 2000.

interesting to note that although there is a lot of interannual variability there is still a statistically significant ($P < 0.01$) slope to the least squares linear fit to this profile (Figure 15).

[35] When the magnitude of the slopes of all anomaly time series are plotted in the 85 by 85 pixel frame, we can visualize the tendency toward positive or negative slopes, and more importantly the spatial coherence amongst and between points in the study area (Figure 16). Over the period 1979 to 2000 the trend in sea ice concentration is toward a reduction (increase in negative ice concentration

anomalies). The spatial pattern of these trends in ice concentrations indicate two distinct regions of reduced concentration (Figure 16): (1) at the interface between the central pack and the landfast ice zone north of the Alaska Coast and in a pattern parallel to the coast line suggesting a process which occurs at or near the shelf break and (2) at the east end of the Cape Bathurst Polynya within Amundsen Gulf. The largest area appears to occur at the interface between the central pack and the fast ice which forms north of Alaska. We speculate that this observation is due mostly to a reduction in the ice



Figure 13. Selected negative concentration anomaly period from the first week in April to the first week in November 1998 expressed as positive and negative sea ice concentration percent relative to the average between 1979 and 2000.

concentration within the central pack or divergence of the pack away from the coast. Local-scale upwelling may support this pattern and teleconnection patterns over the arctic and north pacific may enhance this relationship. This observation is also broadly supported by the AO and sea ice concentration anomaly cross-correlation results presented in Figure 9. The observed reduction in concentra-

tion anomalies in Amundsen Gulf is a bit of a surprise as it will not be related (directly at least) to reductions in the central arctic pack. It may be that the polynya is tending to open earlier and longer or that sea ice may be melting earlier due to atmospheric heat advecting from the landmasses surrounding this region or that local atmospheric flows advect ice out of the region. It is also possible that

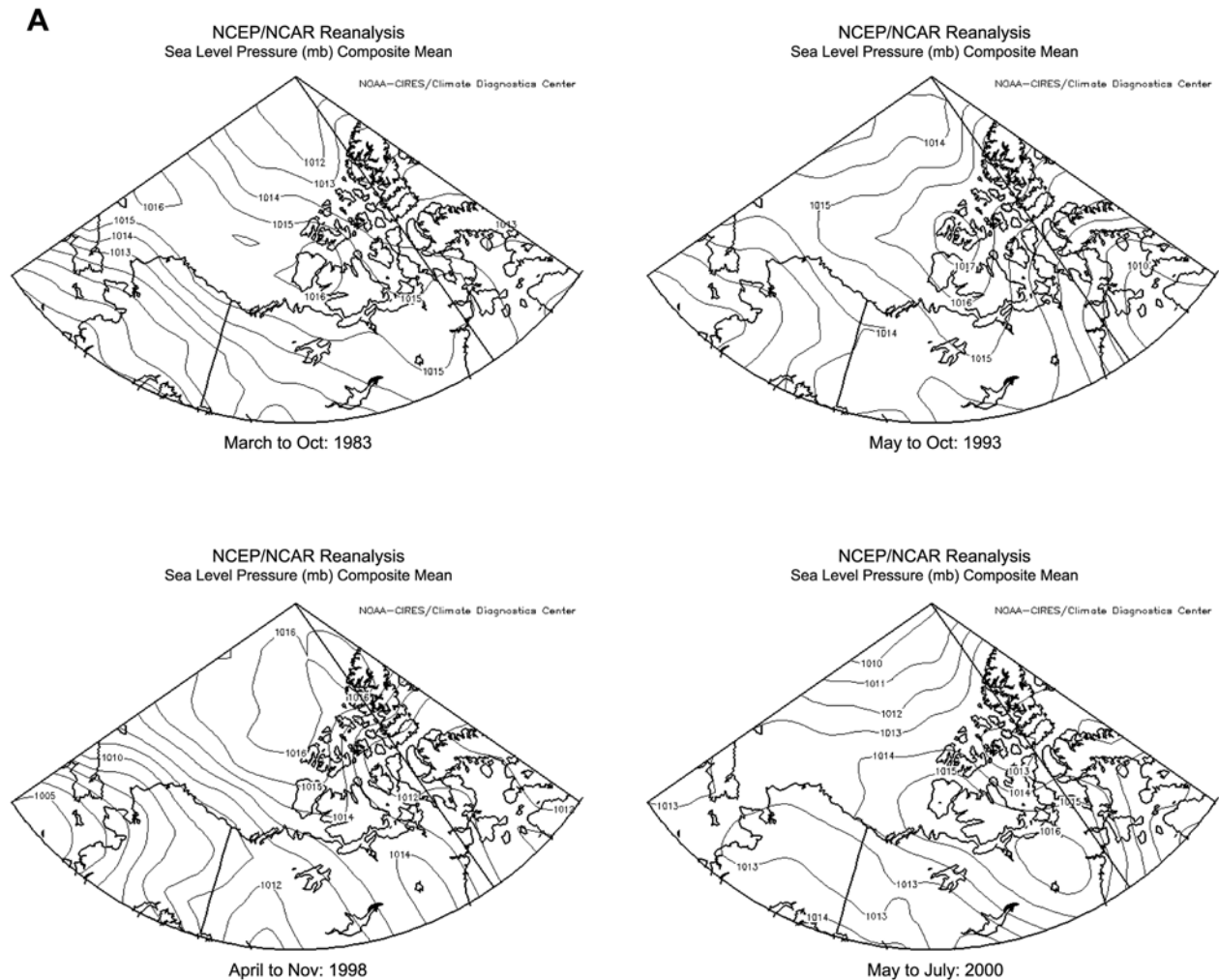


Figure 14. (a) Sea level pressure (SLP - hPa), (b) surface air temperature anomaly ($^{\circ}\text{C}$), and (c) 500 hPa geopotential height anomalies (m) for the positive and negative ice concentration anomalies represented in Figures 8 to 11.

the flaw leads at the shelf break are allowing upwelling of warmer Atlantic water to the base of the sea ice in Amundsen Gulf thereby providing the stimuli for a sensible heat polynya.

[36] Whatever the mechanism, it is apparent that although the CASES study region is experiencing both negative and positive concentration anomalies there is a statistically significant trend toward increasing negative anomalies at least in two distinct subregions of the study area. It is interesting to note that recent work, totally independent of that presented here, has found similar patterns in surface temperature anomalies in these same regions over this same time period [Comiso, 2003].

4. Summary and Conclusions

[37] Our principal motivation for this work has been to examine the coupling between sea ice and the atmosphere, at a range of time and space scales, as a means of setting the context for the Canadian Arctic Shelf Exchange Study (CASES). CASES will examine the details of the physi-

cal-biological coupling in this region over the period 2001 to 2005.

[38] In the study region sea ice growth and decay are a function of both dynamic and thermodynamic processes. The average patterns of both growth and decay show the presence of a persistent polynya in the Cape Bathurst region. The control of the offshore pack on sea ice dynamic processes has been highlighted and the role of freshwater from the Mackenzie in growth and decay of sea ice remains a priority for further research. Although highly variable in both space and time the patterns in sea ice concentration and areal extent show a statistically significant trend toward an increase in negative concentration anomalies throughout the period 1979 to 2000. The spatial pattern of these trends suggest that detailed process analyses should focus attention in two areas: (1) the interface between the central pack and the landfast ice and (2) the Cape Bathurst Polynya complex (including the flaw lead system). These areas are clearly points of high variability in sea ice dynamic and thermodynamic processes and as such are likely places to understand the role of sea ice

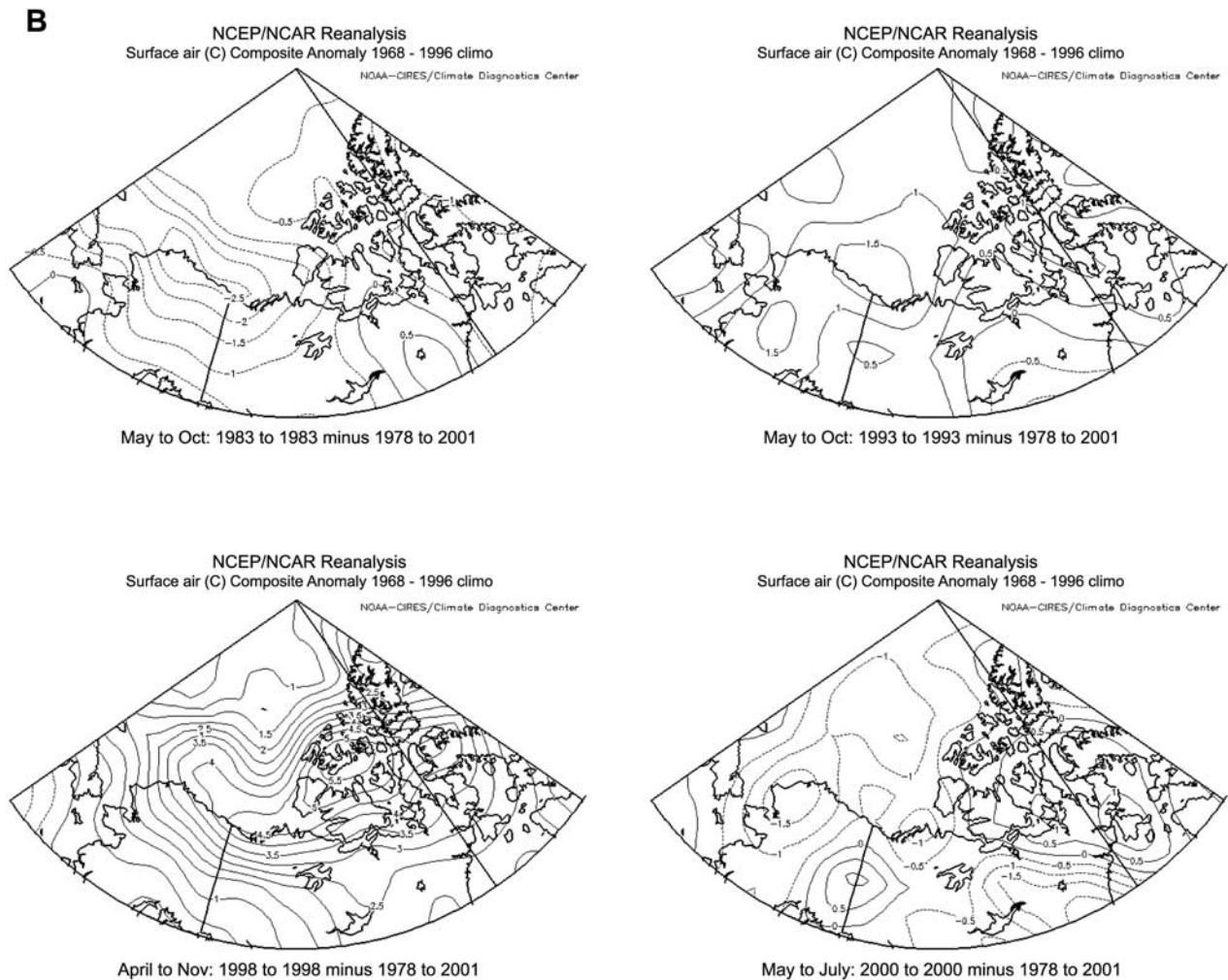


Figure 14. (continued)

variability in dictating the magnitude and timing of biogeochemical fluxes between the Continental Shelf and the Canada Basin.

[39] The processes which drive these observed sea ice patterns appear to be a complex function of local, regional and hemispheric forcing in both the atmosphere and ocean. At the local scale, snow deposition and distribution is important relative to sea ice thermodynamic processes. The role of the ice-albedo feedback in the rates of melt and formation are critical both from the southward advance from the pack ice toward shore and in formation of landfast ice. Although speculative, it would appear that the presence of open water at the shelf break may create conditions suitable for upwelling of warmer Atlantic layer water which may then become available to complicate the thermodynamic growth and decay behavior of the sea ice.

[40] Local-scale winds affect sea ice dynamic and thermodynamic processes through the advection of warmer (colder) air to the region affecting negative (positive) concentration anomalies. Rafting of sea ice due to oceanic or atmospheric forcing can create substantial increases in volume and can affect snow catchment processes. The

role of cyclogenesis will be important throughout the annual cycle as will the frequency and strength of cyclones relative the spatial and temporal patterns of sea ice growth and decay. Clouds will likely have a strong impact on the surface energy balance and are expected to affect both formation and decay of the ice. It is particularly evident that the preconditioning of the sea ice regimes can play a significant role in the annual evolution of the ice cover.

[41] Our results suggest that hemispheric scales may play a significant role in creating the observed sea ice anomalies. A “tighter” polar vortex circulation occurs in years with positive CASES ice anomalies, which is analogous to a positive AO index. This result is broadly consistent with the framework of *Rigor et al.* [2002] in that summer sea ice motion tends to converge toward the southern Beaufort while tending to diverge ice away from the eastern Siberian Shelf. A negative AO in winter will tend to converge ice toward the Siberian Shelf while enhancing divergence away from the southern Beaufort Sea [*Rigor et al.*, 2002]. As with the recent work of *Serreze et al.* [2003] our results are also partially explained by local advection of warmer (colder) air

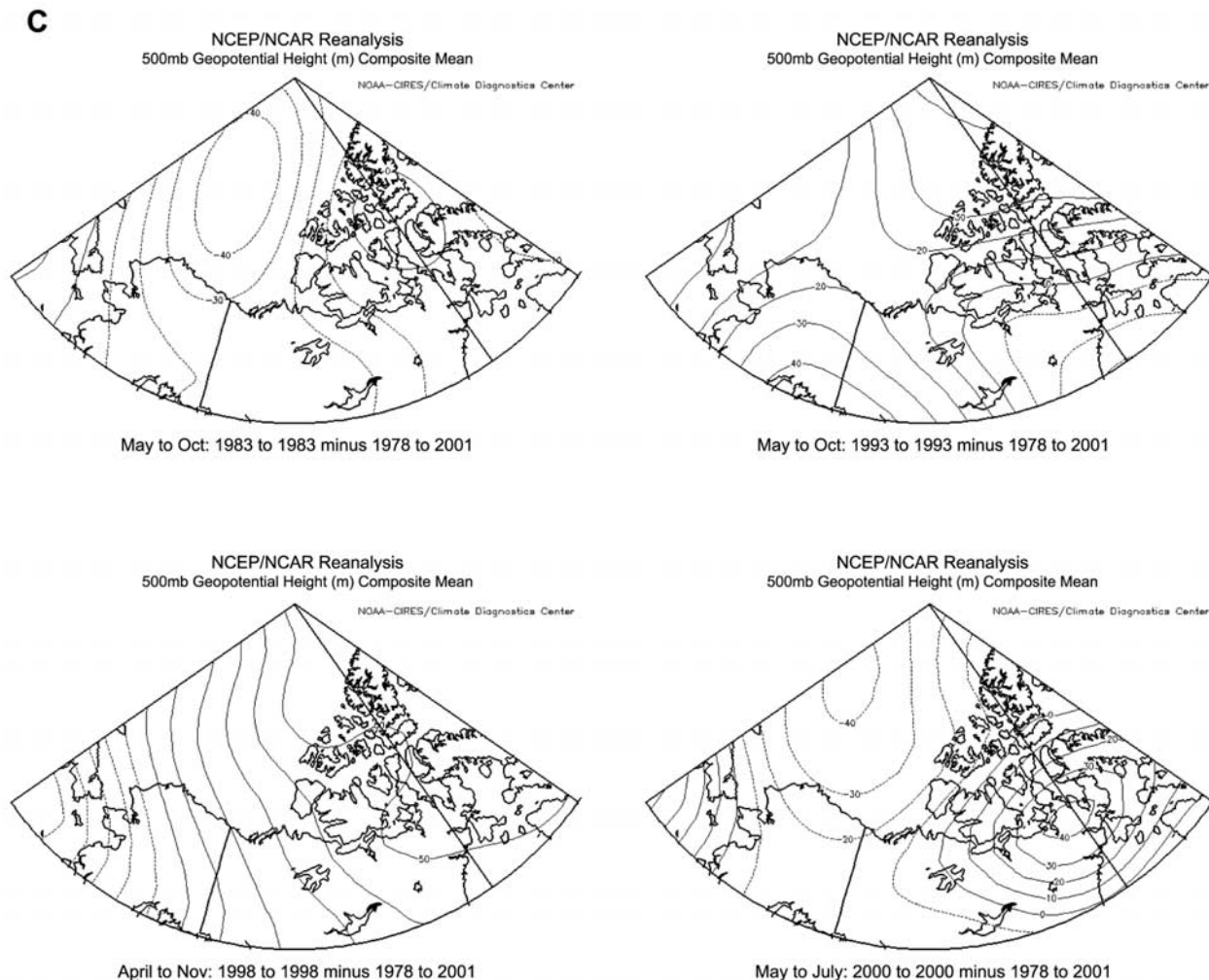


Figure 14. (continued)

masses over the region due to SLP control on surface flow.

[42] The correlation surface (Figure 9) shows the geographic regions where we can expect to find the strongest coupling between sea ice and the AO. These correlations show that about 25 percent of the variance in sea ice concentration anomalies can be attributable to the modes in the AO. High correlation values show the tendency for AO and ice concentration anomalies to be in phase (i.e., both positive or both negative). They also show that geographically the areas most affected by the AO are the CASES study region in the months of May–October and along the northwest coast of the Canadian Archipelago coast, in the winter period (November–April).

[43] It is likely that oceanic and atmospheric forcing work in concert to affect the observed patterns in the sea ice concentration anomalies. Although it is convenient to conceptualize relationships between various ocean and atmospheric connections we need to remember that these indices account for only about 30 percent of the explained variance in surface pressure patterns [e.g., *Thompson and Wallace, 1998*] and that no clear picture yet exists between how the central arctic pack ice responds to changes in the Northern Annular Mode (NAM). It is likely that local-scale atmo-

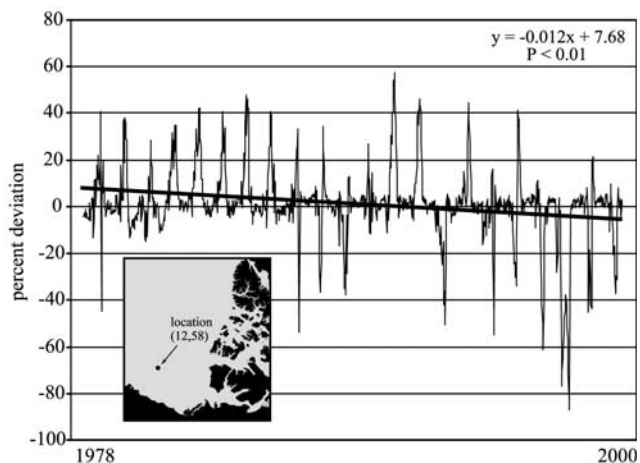


Figure 15. Time series profile of sea ice concentration anomalies for a single pixel located at (12r, 58c). The anomalies are expressed as percent deviation from the average computed between 1979 and 2000 and presented for each week (52) for the 22 years of the data set (22·52) resulting in 1144 data points. The inset shows the geographic location of the pixel and the least squares best fit linear trend is shown to illustrate how the slopes in Figure 16 are computed.

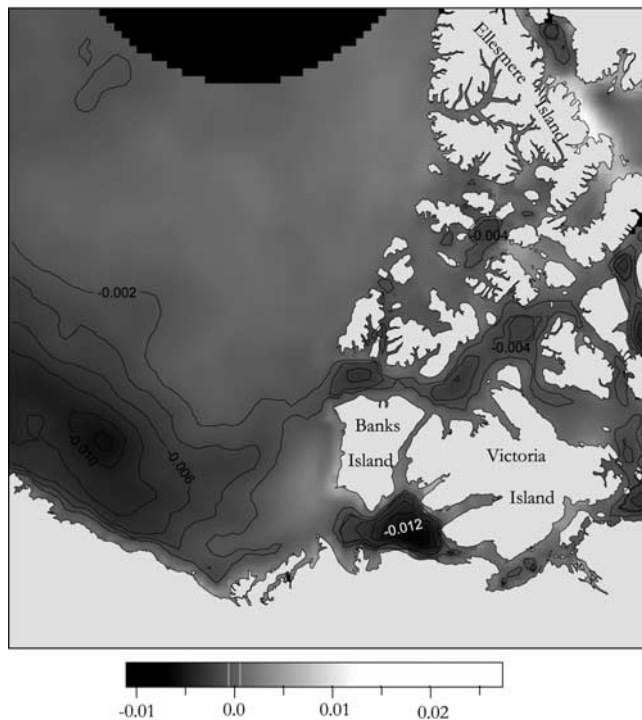


Figure 16. Slopes of the least squares best fit line from each pixel in the data frame based on a statistical analysis of slopes fit through each pixel in the data set (as illustrated in Figure 15). The slopes show trends toward negative (dark) and positive (light) concentration anomalies as a function of spatial location over the period 1979 to 2000. All contours are significant at $\alpha \leq 0.01$.

spheric and oceanic forcing, examined within the context of hemispheric-scale forcing, will lead us to answers regarding the evolution of sea ice concentration, type, and mass in the CASES study region and thereby provide us with a better physical understanding between the coupling of the ocean-sea ice-atmosphere system.

[44] **Acknowledgments.** This work was funded by the Natural Sciences and Engineering Research Council (NSERC) through grants to D. B. and J. H. and to the CASES research network. Some data were provided by the NOAA-CIRES Climate Diagnostics Center, Boulder, Colorado, from their web site at <http://www.cdc.noaa.gov/>. Thanks to NSIDC for providing the passive microwave data and to W. Chan for processing of these data. J. Iacozza, D. Fast, and C. Blouw provided valuable assistance in preparation of the data for this manuscript. This work is a contribution to the Canadian Arctic Shelf Exchange Study (CASES) and the Canadian Cryospheric System (CRYSYS) programs.

References

Agnew, T. A., and S. Howell (2003), The use of operational ice charts for evaluating passive microwave ice concentration data, *Atmos. Ocean*, *41*(4), 317–331.

Barber, D. G., J. Hanesiak, W. Chan, and J. Piwowar (2001), Sea ice and meteorological conditions in northern Baffin Bay and the north water polynya between 1979 and 1996, *Atmos. Ocean*, *39*(3), 343–359.

Barber, D. G., J. Hanesiak, W. Chan, and C. Blouw (2003), An overview of the ocean-sea ice-atmosphere (OSA) system in the CASES study region over the period 1978 to 2001, *CEOS Tech. Rep. CEOS-Tech-03-1*, 80 pp., Cent. for Earth Obs. Sci. (CEOS), Fac. of Environ., Univ. of Manitoba, Winnipeg, Man., Canada.

Carmack, E. C., and R. W. Macdonald (2002), Oceanography of the Canadian Shelf of the Beaufort Sea: A setting for marine life, *Arctic*, *55*, 29–45.

Comiso, J. C. (2003), Warming trends in the Arctic from clear sky satellite observations, *J. Clim.*, *16*, 3498–3510.

Drobot, S. D., and J. A. Maslanik (2003), Interannual variability in summer Beaufort Sea ice conditions: Relationship to winter and summer surface and atmospheric variability, *J. Geophys. Res.*, *108*(C7), 3233, doi:10.1029/2002JC001537.

Emery, W. J., M. Radebaugh, C. W. Fowler, D. Cavalieri, and K. Steffen (1991), A comparison of sea ice parameters computed from advanced very high resolution radiometer and Landsat satellite imagery and from airborne passive microwave radiometry, *J. Geophys. Res.*, *96*, 22,075–22,085.

Emery, W. J., C. Fowler, and J. Maslanik (1994), Arctic sea ice concentrations from special sensor microwave imager and advanced very high resolution radiometer satellite data, *J. Geophys. Res.*, *99*, 18,329–18,342.

Flato, G., and G. J. Boer (2001), Warming asymmetry in climate change simulations, *Geophys. Res. Lett.*, *28*, 195–198.

Holloway, G., and T. Sou (2002), Has Arctic sea ice rapidly thinned?, *J. Clim.*, *15*, 1691–1701.

Hurrell, J. W., Y. Kushnir, and M. Visbeck (2001), The North Atlantic Oscillation, *Science*, *291*, 603–605.

Intergovernmental Panel on Climate Change (2001), *Climate Change: The IPCC Assessment*, edited by J. T. Houghton, G. J. Jenkins, and J. J. Ephraums, Cambridge Univ. Press, New York.

Kalnay, E., et al. (1996), The NCEP/NCAR Reanalysis 40-Year Project, *Bull. Am. Meteorol. Soc.*, *77*, 437–471.

Krahmann, G., and M. Visbeck (2003), Variability of the Northern Annular Mode's signature in Winter sea ice concentration, *Polar Res.*, *22*(1), 51–57.

Kwok, R., and D. A. Rothrock (1999), Variability of Fram Strait ice flux and North Atlantic Oscillation, *J. Geophys. Res.*, *104*, 5177–5189.

Maslanik, J. A., M. C. Serreze, and T. Agnew (1999), On the record reduction in 1998 western Arctic sea-ice cover, *Geophys. Res. Lett.*, *26*, 1905–1908.

Melling, H., and D. A. Riedel (1996), Development of seasonal pack ice in the Beaufort Sea during the winter of 1991–1992: A view from below, *J. Geophys. Res.*, *101*, 1975–1991.

Overland, J. E., and J. M. Adams (2001), On the temporal character and regionality of the Arctic Oscillation, *Geophys. Res. Lett.*, *28*, 2811–2814.

Parkinson, C. L., D. J. Cavalieri, P. Gloersen, H. J. Zwally, and J. C. Comiso (1999), Arctic sea ice extents, areas, and trends, 1978–1996, *J. Geophys. Res.*, *104*, 20,837–20,856.

Proshutinsky, A. Y., and M. A. Johnson (1997), Two circulation regimes of the wind-driven Arctic Ocean, *J. Geophys. Res.*, *102*, 12,493–12,514.

Rigor, I. G., J. M. Wallace, and R. L. Colony (2002), Response of sea ice to the Arctic Oscillation, *J. Clim.*, *15*, 2648–2663.

Rothrock, D. A., Y. Yu, and G. A. Maykut (1999), Thinning of the Arctic Sea ice cover, *Geophys. Res. Lett.*, *26*, 3469–3472.

Serreze, M. C., J. A. Maslanik, T. A. Scambos, F. Fetterer, J. Stroeve, K. Knowles, C. Fowler, S. Drobot, R. G. Barry, and T. M. Haran (2003), A record minimum arctic sea ice extent and area in 2002, *Geophys. Res. Lett.*, *30*(3), 1110, doi:10.1029/2002GL016406.

Steffen, K., and A. J. Schweiger (1990), A multisensor approach to sea ice classification for the validation of DMSP-SSM/I passive microwave derived sea ice products, *J. Photogrammetric Eng. Remote Sens.*, *56*(11), 75–82.

Steffen, K., and A. Schweiger (1991), NASA Team algorithm for sea ice concentration retrieval from Defense Meteorological Satellite Program special sensor microwave imager: Comparison with Landsat satellite imagery, *J. Geophys. Res.*, *96*, 21,971–21,987.

Steffen, K., D. J. Cavalieri, J. C. Comiso, K. St. Germain, P. Gloersen, J. Key, and I. Rubinstein (1992), The estimation of geophysical parameters using passive microwave algorithms, in *Microwave Remote Sensing of Sea Ice*, *Geophys. Monogr. Ser.*, vol. 68, edited by F. Carsey, pp. 243–259, AGU, Washington, D. C.

Thompson, D. W. J., and J. M. Wallace (1998), The Arctic Oscillation signature in the wintertime geopotential height and temperature fields, *Geophys. Res. Lett.*, *25*, 1297–1300.

Vinnikov, K. Y., A. Robock, R. J. Stouffer, J. E. Walsh, C. L. Parkinson, D. J. Cavalieri, J. F. B. Mitchell, D. Garrett, and V. F. Zakharov (1999), Global warming and Northern Hemisphere sea ice extent, *Science*, *286*, 1934–1937.

Visbeck, M., E. Chassignet, R. Curry, T. Delworth, R. Dickson, and G. Krahmann (2003), The ocean's response to North Atlantic variability, in *The North Atlantic Oscillation: Climate Significance and Environmental Impact*, *Geophys. Monogr. Ser.*, vol. 134, edited by J. W. Hurrell et al., pp. 113–145, AGU, Washington, D. C.

D. G. Barber and J. M. Hanesiak, Centre for Earth Observation Science, Faculty of Environment, University of Manitoba, Winnipeg, Manitoba, Canada R3T 2N2. (dbarber@ms.umanitoba.ca)